Comparison between current-voltage measurements and energy band diagrams of metal/p-type cupric oxide contacts

R. López

Tecnológico Nacional de México/Tecnológico de Estudios Superiores de Jocotitlán, Carretera Toluca-Atlacomulco, km 44.8, s/n, Jocotitlán, 50700, Estado de México.

Received 4 December 2024; accepted 9 April 2026

The need to generate ohmic contact between a metal and a semiconductor is fundamental for the development of electronic devices or integrated circuits. The aim of this report is to study the electrical contact between platinum, silver and gold p-type cupric oxide films. Thermal oxidation was carried out on copper sheets at 1000°C for 24 h to grow cupric oxide films. The metal/cupric oxide contacts were fabricated by evaporation of the metals on the surface of the cupric oxide films by the direct-current sputtering method. The crystal structure of the cupric oxide films was determined by the X-ray diffraction technique. Electrical characterization of the metal/cupric oxide films was performed by current-voltage measurements, where, independently of the metal used for the contact, all curves exhibited ohmic behavior. Energy band diagrams of the metal/cupric oxide contact were developed based on the Schottky-Mott model. Current-voltage measurements showed good agreement with the energy band diagrams only for platinum, which was favored by the high value of the work function of platinum. Conversely, the energy band diagrams corresponding to the silver/cupric oxide and gold/cupric oxide contacts, exhibited rectifying behavior. It was suggested that the mismatch between the current-voltage measurements and the energy band diagrams was due to the presence of defects at the surface of cupric oxide films, which led to Fermi level pinning at the CuO surface, making the contact, independent of the work functions.

Keywords: Ohmic contact; cupric oxide; energy band diagrams; metals; I-V curve.

DOI: https://doi.org/10.31349/RevMexFis.72.041006

1. Introduction

Oxidation of copper can lead to the formation of several phases, where the most stable are cuprous oxide (Cu_2O) and cupric oxide (CuO). However, CuO has proven to be thermodynamically more stable than Cu_2O [1]. CuO crystallizes in the monoclinic structure, exhibits a relatively low bandgap of around 1.5 eV, and exhibits intrinsic p-type conductivity [2, 3]. Recently, CuO has been studied for the development of heterojunctions, which have potential applications in solar cells, gas sensors, and degradation of contaminants [4–9]. These applications require that CuO be connected to the "outside world" by electrical contacts, which are formed with several metals, among them: silver (Ag), gold (Au), aluminum (Al), and platinum (Pt) [10–14]. Selection of an appropriate metal can lead to forming an electrical contact with linear behavior, bidirectional current transport, and low power dissipation, which are expected characteristics of an ohmic contact. Although the use of the above-mentioned metals to form ohmic contacts with other semiconductors such as ZnO or TiO_2 is commonly found in the literature, reports about rectifying or ohmic contacts to CuO are scarce. Based on the Schottky-Mott theory, the formation of the type of contact relies on the value of the work functions of both materials. Particularly, the formation of an ohmic contact between a metal and a p-type semiconductor requires a higher work function of the metal than that of the semiconductor. Although CuO is a material with a relatively low bandgap, there are few metals with sufficiently high work functions to form ohmic contacts to CuO. Also, there are some phenomena such as the image-force effect and the Fermi level pinning that can disturb the ideal behavior of the metal/CuO contact. This work aims to analyze the experimental current-voltage behavior of Ag, Au and Pt contacts to CuO films, and compare them with their corresponding energy band diagrams developed by using the Schottky-Mott model.

2. Materials and methods

CuO films were grown by thermal oxidation of metal copper (Cu). Cu sheets (purity of 99.99%, sized to 2×2 cm) were sonicated for 10 min in xylene, then 10 min in acetone, 10 min in ethanol, and finally, they were rinsed in distilled water. The native oxide was removed by sonication of the Cu sheets in a solution containing a 10:1 vol mixture of distilled water and hydrofluoric acid. The Cu sheets were then oxidized in a horizontal tube furnace (EVELSA CMOD-HAT-1100-D25) at 1000°C for 24 h in an ambient atmosphere with an air flow-rate of 200 standard cubic centimeters per minute. The CuO films were cooled down to room temperature naturally. Structural measurements by X-ray diffraction (XRD) were done by using a Bruker diffractometer model D8 Discover with a CuKα radiation of 1.54 Å. Electrical contacts of the CuO films were deposited by the DC sputtering method using an auto-sputter coater, Agar 108 A, performing three cycles of 5 minutes for deposition of each metal. The metals evaluated were Pt, Ag and Au, and were deposited at the ends of the surface of the CuO films, leaving a free space

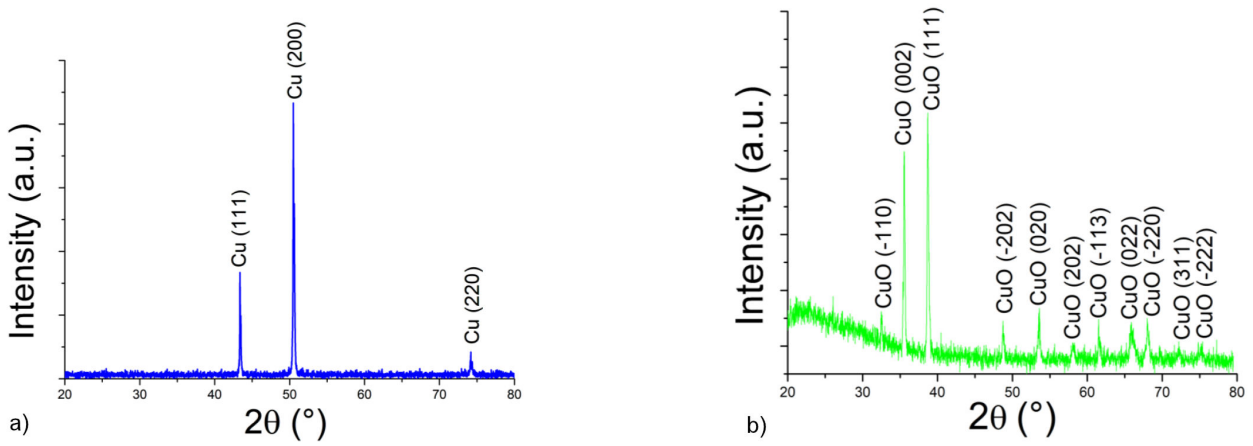

FIGURE 1. XRD diffractograms of the: a) Cu sheet, and b) CuO film grown by thermal oxidation of Cu.

of 1 cm between the metals. Current-voltage (I-V) measurements were performed using a source-measure unit system Keithley 2450. The electrical resistance was measured by the two-point method using a digital multimeter STEREN, model MUL-600.

3. Results and discussion

3.1. XRD measurements

XRD patterns of Cu sheets and CuO films are shown in Fig. 1. The three peaks observed in the XRD pattern of the Cu sheet [Fig. 1a)], correspond to those characteristics of the crystalline metal Cu ((111), (200), and (220), PDF file 00-004-0836). Peaks corresponding to the copper oxide phase were not found. Figure 1b) shows the XRD pattern of the CuO film where nine peaks can be observed. These peaks correspond sequentially from the left to the right, respectively, to the (-110), (-111), (111), (-202)(020),(202),(-113)(-311), and (-220), planes of the CuO phase (PDF file 00-045-0937). No peaks of the metal copper or other copper oxide phases were found in the XRD pattern, indicating a full oxidation of the surface of the Cu sheet and crystallization of a single phase of copper oxide.

3.2. I-V characterization

The I-V curves of the Pt/CuO/Pt, Ag/CuO/Ag, and Au/CuO/Au contacts are shown in Fig. 2a). The three curves are linear, indicating that the three metals formed ohmic contacts with the semiconductor CuO. Figures 2b), 2c), and 2d), show the experimental array of the electrodes for the measurements of the I-V curves for each metal/CuO contact. Indirectly, the highest value of the slope of the I-V curve of the Au/CuO contact suggests that, among the three contacts studied here, it formed the best electrical contact as it exhibits the highest values of electrical current under the applied voltages. According to the Ohm's law and by using the values of the slopes, the electrical resistance (ER) values of each metal/CuO contact can be obtained by using the two-point probe method. The ER value is dependent upon different features of the contact such as the geometry of the sample, contact surface, and experimental array of the measurement; however, once the graph of the I-V curve exhibits a linear characteristic in direct and reverse polarization, and setting up an identical experimental array for the two-point probe method, the value of the ER can be used as a first approximation for identifying the best ohmic contact among several samples (Table I). The range of the ER is found in kΩ, and it was reduced from the Pt/CuO/Pt, then to the Ag/CuO/Ag, and finally with the Au/CuO/Au contact. In fact, the ER of the Ag/CuO/Ag contact is more than twice the value of the ER of the Au/CuO/Au and the ER of the Pt/CuO/Pt contact is almost four times that of the Au/CuO/Au.

3.3. Band diagrams

For developing the energy band diagrams of the metal/semiconductor contact, several parameters of the metals and of the CuO are needed. The work function (ϕ) of the metals Pt (ϕ_{Pt}), Ag (ϕ_{Ag}), and Au (ϕ_{Au}), are, 5.7, 4.26 and

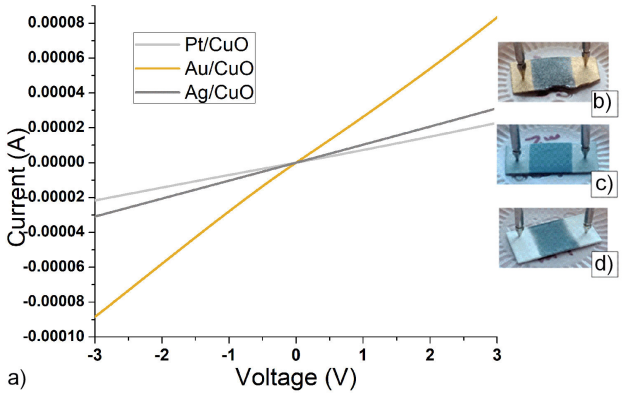

FIGURE 2. I-V characterization of the Pt/CuO/Pt, Ag/CuO/Ag, and Au/CuO/Au contacts. a) I-V curves, b), c), and d), illustrative photographs of the experimental array performed for the I-V characterization.

TABLE I. Electrical resistance (ER) of the three studied metal/CuO contacts, obtained from the I-V curve by the two-point probe method.

Sample	Electrical resistance (kΩ)
Pt/CuO/Pt	136.419
Ag/CuO/Ag	98.156
Au/CuO/Au	35.531

and 5.1, respectively [15]. The band gap (Eg), the acceptor concentration (Na), the electron affinity (χ_{CuO}), the position of the Fermi level measured from the valence band (δ_p), and the work function (ϕ_{CuO}), previously obtained for the CuO films were: 1.51 eV, 9.54×10^{12} cm^{-3}, 4.07 eV, 0.46 eV, and 5.12 eV, respectively [16, 17]. According to the Schottky-Mott theory, when an electrical contact is performed between a metal and a p-type semiconductor, it is ohmic if the $\phi_{\text{metal}} > \phi_{\text{semiconductor}}$, and it is rectifying if the $\phi_{\text{semiconductor}} > \phi_{\text{metal}}$ [18, 19]. Based on this model, the fabrication of ohmic contacts is difficult due to the ϕ of most metals is under 6 eV and some semiconductors exhibit wide-bandgaps. The energy band diagram of Pt and CuO before the contact (left of Fig. 3), shows how the difference between the value of the work functions ($\phi_{\text{Pt}} > \phi_{\text{CuO}}$), supports the formation of an ohmic contact. When these materials are brought in contact, valence electrons from the surface of the semiconductor CuO will move to the metal Pt ("holes move from the metal to the surface of the semiconductor, at the valence band"), leaving holes back; and thus, when the system reaches thermal equilibrium, there is a hole accumulation at the surface of CuO, making it more p-type. This "hole injection from the metal" makes CuO more p-type at the surface, which is depicted by an upward band bending at the junction (the valence band is closer to the Fermi level) (right of Fig. 3). The built-in voltage (Vbi) is, in a rectifying contact (metal/p-type semiconductor where $\phi_{\text{semiconductor}} > \phi_{\text{metal}}$), the barrier seen by holes trying to move from the semiconductor (CuO) into the metal (Pt). The difference between $\phi_{\text{semiconductor}}$ and the ϕ-metal represents the total downward band bending of the valence band at the surface of the semiconductor. In contrast, for an ohmic contact, as commented above, the accumulation of holes at the surface of the semiconductor is illustrated by the upward band bending. Thus, when a positive voltage is applied to the semiconductor, there is no barrier for holes trying to move from the semiconductor to the metal. The theoretical barrier height (ϕ_{bp}), also known as the Schottky barrier, is for a metal/p-type semiconductor, the barrier seen by "holes trying to move from the metal to the semiconductor" (barrier seen by electrons in the valence band of the semiconductor trying to move to the metal). This barrier should be as low as possible to develop a good ohmic contact. The ϕ_{bp} for the Pt/p-type CuO contact can be obtained as in Eq. (1) [20, 21]:

$$\phi_{bp} = (Eg_{\text{CuO}} + \chi_{\text{CuO}}) - \phi_{Pt}. \tag{1}$$

The ϕ_{bp} is measured from the Fermi level to the maximum of the valence band at the junction, which in a rectifying contact, is the sum of δ_p (at the bulk) plus V_{bi}. On the other hand, for an ohmic contact, the higher value of ϕ_{metal} compared to the $\phi_{\text{semiconductor}}$ not only results in an upward band bending in the semiconductor side but also makes ϕ_{bp} very low or even negative. Thus, $\phi_{bp} = -0.12$ eV for the Pt/CuO contact. This low ϕ_{bp} symbolizes a "very low barrier seen by holes trying to move from Pt to CuO" (very low barrier seen by electrons in the valence band of CuO trying to move to Pt). The total upward band bending in the Pt/CuO ohmic

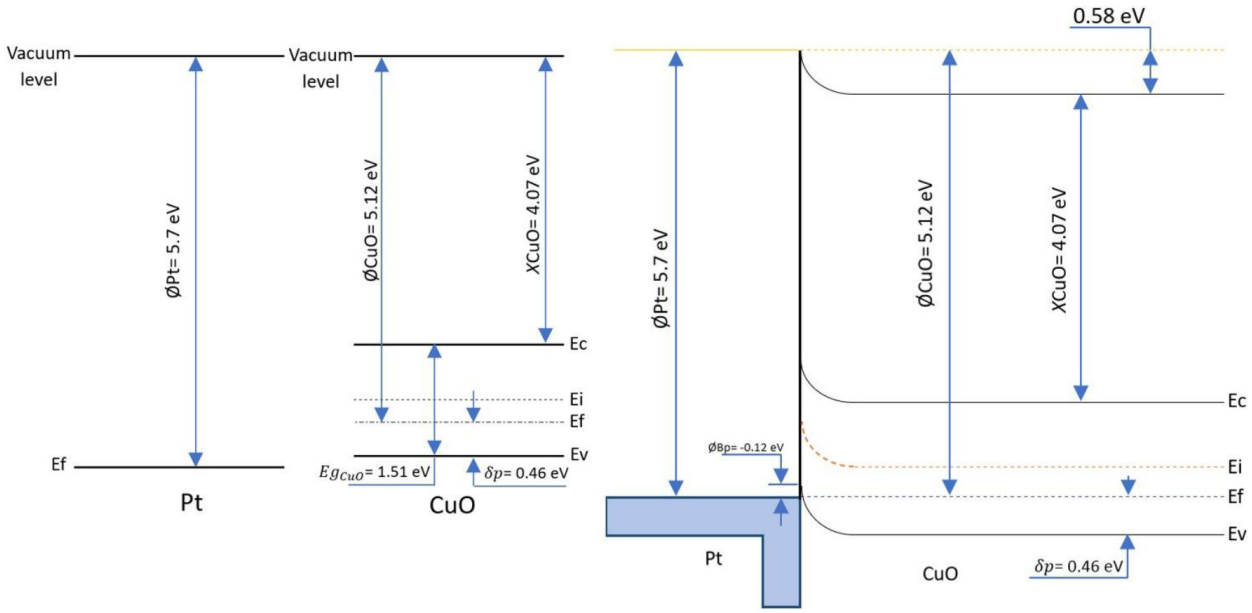

FIGURE 3. Ideal energy band diagrams of the Pt/p-CuO; before the contact (left), and under thermal equilibrium (right).

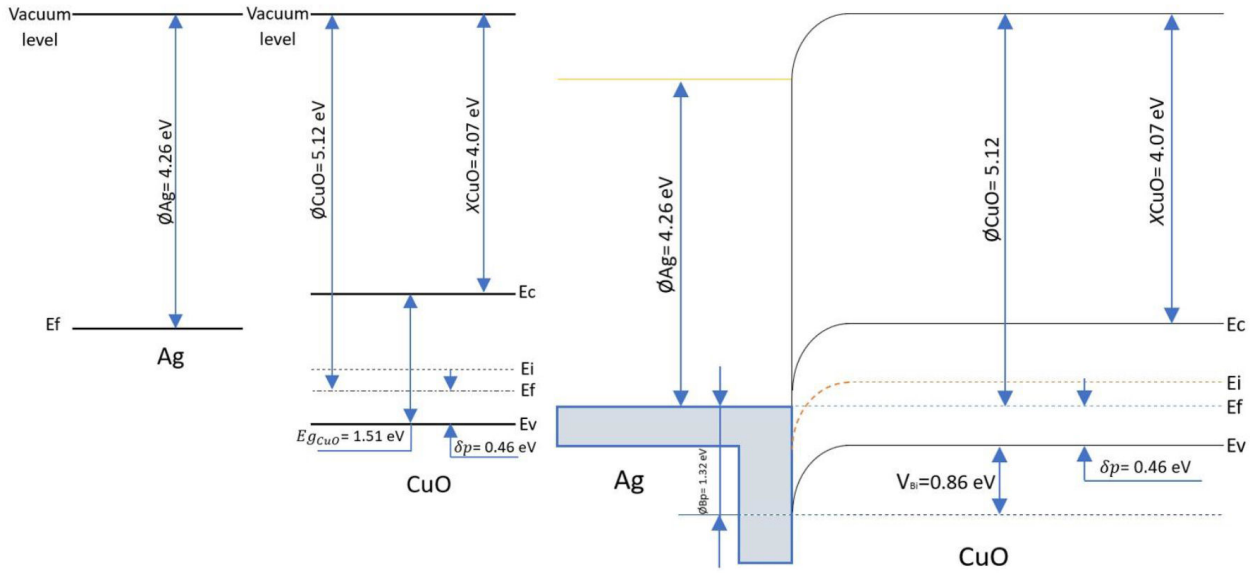

FIGURE 4. Ideal energy band diagrams of the Ag/p-CuO; before the contact (left) and under thermal equilibrium (right).

contact is equal to the sum of $\delta_p + \phi_{bp} = 0.58$ eV. The energy band diagram of the Pt/CuO contact supports a first-order approximation of the ohmic contact under thermal equilibrium condition, without application of an external electric field.

Based on the Schottky-Mott model and considering that the $\phi_{\rm Ag}$ is lower than that of CuO (left of Fig. 4), the Ag/CuO contact should exhibit a rectifying behavior. The complementary parameters required for the development of the energy band diagram of the Ag/CuO contact are $\phi_{bp} = 1.32$ eV, and $V_{bi} = 0.86$ eV. The corresponding energy band diagram is shown at the right of Fig. 4. When the contact is made, the bands are downward (the Fermi level moves away from the valence band) due to there is a depletion of holes at the surface of CuO promoted by electrons moving from Ag to the valence band of CuO ("holes from the semiconductor move to the metal Ag"), completing bonds by occupying "free spaces" (holes).

It is interesting to note that the low value of $\phi_{\rm Ag}$ induced a high value of V_{bi}, limiting the hole transport across the junction, which macroscopically is observed as a high value of the electrical resistance. This effect can be analyzed under reverse polarization of the Ag/CuO contact (a positive voltage applied to Ag in relation to CuO). That is, in the idealized case where ϕ_{bp} remains constant, the increase of the applied voltage will induce an increase in the barrier height that holes see when they try to move from the semiconductor to the metal, due to electrons injected from the negative electrode of the power source (at the CuO side) can "fill" the holes placed near the depletion region of CuO, increasing the width of it. There is a mismatch between the I-V curve [Fig. 2a)] and the corresponding energy band diagram of the Ag/CuO contact, where the first, which is an experimental measurement, exhibited an ohmic curve, while the theoretical model suggested a rectifying behavior. Although direct evidence of interface states was not measured, the observed independence of contact behavior from metal work function strongly suggests Fermi level pinning at the CuO surface. The mechanism governing the carrier transport across the interface of a metal/semiconductor contact can be estimated by comparison between the Stratton-Padovani parameter (also known as the tunneling parameter and dependent upon the carrier concentration) E_{00}, and the value of the thermal energy at room temperature $kT = 0.0259$ eV [20]. The mechanism is supported by thermionic emission if $E_{00} \ll kT$, which matched well for the CuO samples, due to $E_{00} = 0.00629$ meV. It is known that for tunneling transport at the interface between the metal and the semiconductor, it is necessary to use a highly doped semiconductor, which for CuO requires at least an acceptor concentration of 10^{19} cm^{-3} [22] . Thus, hole-tunneling across the Ag/CuO interface is ruled out due to the low acceptor concentration in the CuO samples (10^{12} cm^{-3}). Thus, there are two interesting effects observed for the Ag/CuO contact: one is that its ohmic behavior firstly indicates a strong independence of the work functions, even when the difference between $\phi_{\rm Ag}$ and $\phi_{\rm CuO}$ is relatively high. The other is that, based on the energy band diagram, under reverse polarization, the holes should be "easily" transported from the semiconductor to the metal over the "high" potential barrier V_{bi}. These effects can be explained by the presence of surface defects at the side of CuO, which "pin" the Fermi level and give rise to the following: independently of the metal used for the contact, for n-type semiconductors this leads to rectifying behavior while for p-type semiconductors, it leads to ohmic behavior [23].

Finally, the energy band diagram for the Au/CuO contact can be drawn by considering the $\phi_{\rm Au}$, which is 5.1 eV. Rigorously, the Au/CuO contact should be rectifying due to $\phi_{\rm CuO} > \phi_{\rm Au}$. Thus, $\phi_{bp} = 0.48$ eV and $V_{bi} = 0.02$ eV. Figure 5 shows the energy band diagrams of Au and CuO before and after the contact. A comparison between the value of

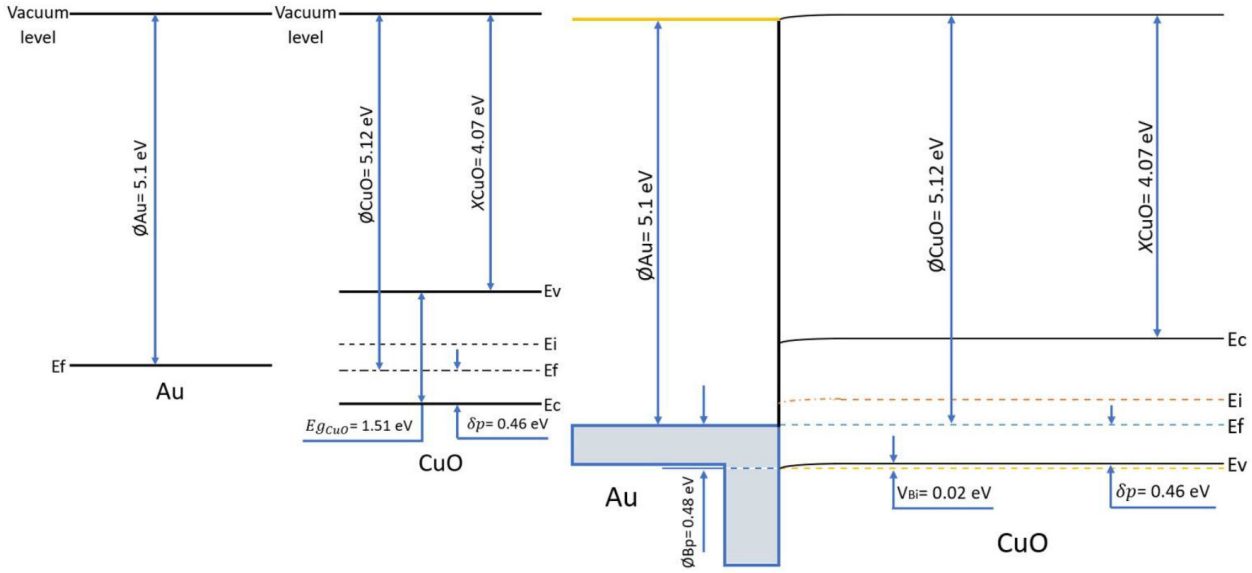

FIGURE 5. Ideal energy band diagrams of the Au/p-CuO contact; before the contact (left) and under thermal equilibrium (right).

of ϕ_{bp} for Ag $=$ 1.32 eV and ϕ_{bp} for Au $=$ 0.48 eV, indicates a lower threshold or activation voltage for a rectifying Au/p-CuO device under forward polarization (a positive voltage applied to the semiconductor in relation to the metal). Conversely, under reverse polarization, the low value of $V_{bi} = 0.02$ eV, initially indicates a narrower depletion region than that for the Ag/CuO contact. However, the effect of increasing the voltage under reverse polarization will induce an increase in the width of the depletion region, which similar to the Ag/p-CuO contact, will make difficult the hole transport across the interface between Au and CuO. However, the experimental behavior observed through the I-V curve was ohmic for the Au/CuO contact. Newly, the energy band diagram of Fig. 5 does not consider the effects of surface states, which could lead to the pinning of the Fermi level. Although CuO is a material not much explored in terms of metal/semiconductor contacts, Morasch and coworkers studied the ohmic contact between Au and p-type CuO thin films with a bandgap of 1.5 eV and an acceptor concentration of 10^{20} cm^{-3} [24]. They found that the Fermi level is very close to the valence band due to chemical reduction of CuO when it makes contact with Au, which places Au as a perfect metal to fabricate ohmic contacts to CuO.

4. Conclusions

The study of the electrical contacts between Pt, Ag and Au to p-CuO was made by comparing the experimental I-V curves with the Schottky-Mott-based energy band diagrams. Only the Pt/CuO contact matched well between the experimental behavior and the theoretical model, because Pt has one of the highest work functions among metals. Conversely, for Ag and Au, the I-V curve exhibited ohmic behaviors for the contacts formed to CuO, although their energy band diagram proposed a rectifying behavior. This effect was explained based on the Fermi level pinning effect.

Author contributions

Roberto López: Conceptualization, Methodology, Software, Formal analysis, Validation, Writing-original draft, Writing-review & editing.

Funding

This research did not receive any specific grant.

Declarations

Competing interests

The author reports no declarations of interest

1. S. Steinhauer, Gas sensors based on copper oxide nanomaterials: *A review, Chemosensors* **9** (2021) 51, https://doi.org/10.3390/chemosensors9030051
2. E. Arulkumar and S. Thanikaikarasan, Structure, morphology, composition, optical properties and catalytic activity of nanomaterials CuO, NiO, CuO/NiO using methylene blue, *Optik* **302** (2024) 171685, https://doi.org/10.1016/j.ijleo.2024.171685
3. W. Lu *et al.*, Ag nanoparticles-decorated p-type CuO/n-type ZnO heterojunction nanofibers with enhanced photocat-

alytic activities for dye degradation and disinfection, *J. Alloy Compd.* **968** (2023) 171864, https://doi.org/10.1016/j.jallcom.2023.171864

4. T.F. Yadeta and T. Imae, Effect of carbon dot on photovoltaic performance of n-TiO_2/p-NiO and n-TiO_2/p-CuO heterojunctions in dye-sensitized solar cells, *Appl. Surf. Sci.* **637** (2023) 157880, https://doi.org/10.1016/j.apsusc.2023.157880

5. N. Jahan *et al*., A comparative study of CuO based solar cell with ZnTe HTL and SnS_2 ETL using SCAPS 1D simulation, *J. Opt.* **54** (2025) 952 https://doi.org/10.1007/s12596-024-01800-6

6. J. Yang, T. Wang, C. Zhu, X. Yin, P. Dong, and X. Wu, AgNWs@SnO_2/CuO nanocomposites for ultra-sensitive SO_2 sensing based on surface acoustic wave with frequency-resistance dual-signal display, *Sensor. Actuat. B-Chem.* **375** (2023) 132966, https://doi.org/10.1016/j.snb.2022.132966

7. K. Bano, S. Kaushal, B. Lal, S.K. Joshi, R. Kumar, and P.P. Singh, Fabrication of CuO/ZnO heterojunction photocatalyst for efficient photocatalytic degradation of tetracycline and ciprofloxacin under direct sunlight, *Environ. Nanotechnol. Monit. Manag.* **20** (2023) 100863, https://doi.org/10.1016/j.enmm.2023.100863

8. A. Sreedhar and J.S. Noh, Ti_3C_2 MXene interfaced ZnO/CuO heterojunction for superior visible light PEC water splitting, *Ceram. Int.* **50** (2024) 37754, https://doi.org/10.1016/j.ceramint.2024.07.138

9. N.H. Touidjen, M. Lamri Zeggar, M.S. Aida, S. Rouabah, and N. Aouabdia, Volatile organic compound gas sensing applications of n-type SnO_2 and p-type CuO based on thin films, *J. Electron. Mater.* **53** (2024) 515, https://doi.org/10.1007/s11664-023-10559-8

10. M. Ma *et al.*, Revealing the crucial role of skeleton restructuring on erosion dispersion of Ag–CuO contact materials, *Appl. Surf. Sci.* **611** (2023) 155676, https://doi.org/10.1016/j.apsusc.2022.155676

11. K. Abdelkarem, R. Saad, A.M. Ahmed, M.I. Fathy, M. Shaban, and H. Hamdy, Efficient room temperature carbon dioxide gas sensor based on barium doped CuO thin films, *J. Mater. Sci*. **58** (2023) 11568, https://doi.org/10.1007/s10853-023-08687-x

12. X. Zeng, M. Zhukova, S. Faniel, G. Li, and D. Flandre, Properties and aging of bottom-contact CuO/Au transmission line model (TLM) structures, *IEEE T. Electron Dev.* **71** (2024) 6254, https://doi.org/10.1109/TED.2024.3441565

13. T. Bajpai, A.K. Dwivedi, S. Tripathi, L. Agrawal, and S. Tripathi, CuO and MoS_2 nanocomposite-based high-performance wideband photodetector, *IEEE T. Electron Dev.* **71** (2024) 6799, https://doi.org/10.1109/TED.2024.3462657

14. D. Mahana, R. Yadav, P. Singh, S. Husale, and S.K. Muthusamy, Photo-sensing characteristics of CuO thin films synthesized by thermal oxidation of Cu metal films, *Opt. Mater.* **148** (2024) 114903, https://doi.org/10.1016/j.optmat.2024.114903

15. H.B. Michaelson, The work function of the elements and its periodicity, *J. Appl. Phys.* **48** (1977) 4729, https://doi.org/10.1063/1.323539

16. R. López *et al*., Cupric oxide (CuO)/zinc oxide (ZnO) heterojunction diode with low turn-on voltage, *Results Phys.* **22** (2021) 103891, https://doi.org/10.1016/j.rinp.2021.103891

17. F.P. Koffyberg and F.A. Benko, A photoelectrochemical determination of the position of the conduction and valence band edges of p-type CuO, *J. Appl. Phys.* **53** (1982) 1173, https://doi.org/10.1063/1.330567

18. W. Schottky, Halbleitertheorie der Sperrschicht, Naturwissenschaften **26** (1938) 843, https://doi.org/10.1007/BF01774216

19. N.F. Mott, Note on the contact between a metal and an insulator or semiconductor, *Math. Proc. Cambridge* **34** (1938) 568, https://doi.org/10.1017/S0305004100020570

20. L. Huang, M. Xia, and X. Gu, A critical review of theory and progress in ohmic contacts to p-type SiC, *J. Cryst. Growth* **531** (2020) 125353, https://doi.org/10.1016/j.jcrysgro.2019.125353

21. K.C. Kao, Electrical conduction and photoconduction, in: Dielectric Phenomena in Solids, Academic Press, California, USA (2004) 381-514, https://doi.org/10.1016/B978-012396561-5/50017-7

22. J. Deuermeier *et al*., Visualization of nanocrystalline CuO in the grain boundaries of Cu_2O thin films and effect on band bending and film resistivity, *APL Mater.* **6** (2018) 096103, https://doi.org/10.1063/1.5042046

23. R.R. Lieten, S. Degroote, M. Kuijk, and G. Borghs, Ohmic contact formation on n-type Ge, *Appl. Phys. Lett.* **92** (2008) 022106, https://doi.org/10.1063/1.2831918

24. J. Morasch, H.F. Wardenga, W. Jaegermann, and A. Klein, Influence of grain boundaries and interfaces on the electronic structure of polycrystalline CuO thin films, *Phys. Status Solidi A* **213** (2016) 1615, https://doi.org/10.1002/pssa.201533018